THYROID
Volume 23, Number 10, 2013

DOI: 10.1089/thy.2013.0037

The PLK1 Inhibitor GSK461364A Is Effective in Poorly Differentiated and Anaplastic Thyroid Carcinoma Cells, Independent of the Nature of Their Driver Mutations

Marika A. Russo, Kristy S. Kang, and Antonio Di Cristofano

Background: Poorly differentiated thyroid carcinoma (PDTC) and anaplastic thyroid carcinoma (ATC) are the most aggressive forms of thyroid cancer. Despite their low incidence, they account for a disproportionate number of thyroid cancer–related deaths because of their resistance to most therapeutic approaches. We have generated mouse models that develop ATC ([*Pten*, *p53*]$^{thyr-/-}$ mice) and follicular thyroid cancer with areas of poor differentiation (*Pten*$^{thyr-/-}$,*Kras*^{G12D} mice). Comparative gene expression profiling of human and mouse ATCs reveals a common "mitotic signature" in which mitotic kinases, including Polo-like kinase-1 (PLK1), are found deregulated in both species. Most genes from this signature are also upregulated in poorly differentiated tumors developing in *Pten*$^{thyr-/-}$,*Kras*^{G12D} mice. PLK1 is a crucial driving force for normal mitotic spindle formation, centrosome maturation, and separation, and its overexpression has been demonstrated in a wide range of tumors.
Methods: Human and mouse ATC and PDTC cell lines were treated with the PLK1 inhibitor GSK461364A, and proliferation, apoptosis, and mitotic spindle alterations were analyzed. Furthermore, immunocompetent mice were injected in the flank with mouse ATC cells, and treated with placebo or GSK461364A.
Results: We show that the PLK1 inhibitor GSK461364A inhibits cell proliferation and induces cell death in both mouse ATC- and PDTC-derived cell lines and in several human ATC cell lines carrying different driver mutations. Dose-dependent changes in chromosome alignment and spindle assembly during mitosis are observed after treatment, together with changes in the mitotic index. FACS analysis reveals a G2/M phase arrest, followed by apoptosis, and mitotic slippage in cells with PI3K activation. GSK461364A is also effective *in vivo*, in an allograft model of ATC.
Conclusions: Taken together, these data suggest that PLK1 targeting is a promising and effective therapeutic approach against PDTC cells and undifferentiated thyroid carcinoma cells.

Introduction

Anaplastic thyroid carcinomas (ATCs) and poorly differentiated thyroid carcinomas (PDTCs) can arise *de novo* or derive from pre-existing differentiated thyroid tumors (1–3). ATC and PDTC presentation at diagnosis is typically advanced, with local invasion of the neck soft tissues, airway compromise, lymph node involvement, and distant metastasis (3,4). These characteristics make most ATCs surgically unresectable and thus one of the most lethal tumor types, with a median survival of less than 6 months (5). To date, no effective therapeutic regimens exist for ATC. Traditional cytotoxic chemotherapies, such as doxorubicin and paclitaxel, are highly toxic and largely ineffective at prolonging survival in ATC patients (6–8). Results from a phase II trial with paclitaxel showed a short-term 53% total response rate, but no change in disease outcome (8). Radiation therapy, alone or in conjunction with doxorubicin, has not shown any improvement in overall survival (6). The poor outcome of chemotherapy is in part linked to the elevated levels and activity of multidrug-resistant proteins (9), strong activation of pro-survival pathways, and a high degree of chromosomal instability and aneuploidy (10).

Although PDTC bears a slightly better prognosis, therapy-refractory metastatic disease is common (>50%) and often results in death (11).

Up to 80% of human ATCs display loss or inactivation of *TP53* (12), whereas in over 40% the PI3K cascade is

Department of Developmental and Molecular Biology, Price Center for Genetic and Translational Medicine, Albert Einstein College of Medicine, Bronx, New York.

constitutively activated through mechanisms that include *PTEN* loss and *PIK3CA* amplification or mutation (13). Additional common driver oncogenic mutations include *BRAF* (2) and *RAS*-activating mutations (14).

We have generated the first autochthonous and immunocompetent mouse model of ATC by combining loss of *p53* and PI3K activation in the thyroid follicular cells (15). The [*Pten*, *p53*]$^{thyr-/-}$ ATC mouse model closely recapitulates human ATC: tumors developing in the compound mutants display histological characteristics similar to those seen in human tumors, elevated genomic instability, and aneuploidy (15). These tumors are highly aggressive, invasive, and metastasize in about 30% of cases.

Polo-like kinase-1 (PLK1) is an essential mitotic regulator found overexpressed in many tumor types, including breast, colorectal, endometrial, ovarian, and pancreatic cancer (16). Overexpression of PLK1 is correlated with constitutive AKT activation (17). PLK1 strongly promotes the progression of cells through mitosis and actively participates in a number of processes that are crucial in multiple stages of mitosis, including mitotic entry, centrosome maturation, bipolar spindle formation, chromosome segregation, cytokinesis, and mitotic exit (18). PLK1 dynamically localizes to various mitotic structures as cells progress through different stages of mitosis [reviewed in (19)].

Several PLK1 inhibitors have been studied in clinical trials with promising results (20–23), and new compounds are in preclinical development (24,25).

Gene expression profiling has dramatically altered the field of cancer cell biology, identifying many genes that play a role in carcinogenesis, and providing key preliminary observations that have led to the design of novel targeted therapeutic approaches (26). Our comparative analysis between mouse and human ATC expression datasets has highlighted a high number of common deregulated genes and pathways, including a mitosis-centered network (15).

The presence of Plk1 as one of the central nodes in the mitotic network found deregulated in [*Pten*, *p53*]$^{thyr-/-}$–derived ATCs prompted us to test whether Plk1 inhibitors would be effective against mouse ATC cell lines. GSK461364A, an imidazotriazine, is an antiproliferative agent *in vitro* and in multiple *in vivo* tumor models, and has been evaluated in a phase I study in patients with advanced solid tumors (20). As a competitive ATP kinase inhibitor, GSK461364A is highly specific for PLK1 (Ki $\leq$0.5 nM compared with 860 and 1000 nM for PLK2 and PLK3, respectively). It induces mitotic arrest with the hallmark of polo spindle morphology in tumor cells, and it inhibits proliferation of cancer cell lines from multiple origins with minimal toxicity in nondividing human cells (27).

Here we have tested the activity of this inhibitor in cell lines derived from [*Pten*, *p53*]$^{thyr-/-}$ mouse ATCs, in PDTC cell lines derived from the *Pten*$^{thyr-/-}$,*Kras*^{G12D} mouse model (28,29), as well as in a panel of genetically annotated human ATC cell lines representing the most common mutational landscape of this tumor type.

Materials and Methods

Establishment and maintenance of cell lines

Primary thyroid tumors from [*Pten*, *p53*]$^{thyr-/-}$ mice were minced and resuspended in Ham's F12/10% fetal bovine serum (FBS) with 100 U/mL type I collagenase (Sigma-Aldrich, St. Louis, MO) and 1 U/mL dispase (Roche Applied Science, Indianapolis, IN). Enzymatic digestion was carried out for 90 minutes at 37°C. After digestion, cells were seeded in Ham's F12 containing 40% Nu-Serum IV (Collaborative Biomedical, Bedford, MA), gly-his-lys (10 ng/mL; Sigma-Aldrich), and somatostatin (10 ng/mL; Sigma-Aldrich) and allowed to spread and reach confluence before being passaged. After the fourth passage, tumor cells were adapted to grow in Dulbecco's modified Eagle's medium/10% FBS. T683 and T826 cell lines were established from poorly differentiated tumors arising in *Pten*$^{thyr-/-}$, *Kras*^{G12D} mice (29).

Human cell lines were grown in Dulbecco's modified Eagle's medium/10% FBS (ACT-1, 8505c) or RPMI/10% FBS (CAL62, C643, OCUT-2, and THJ16T). All cell lines were validated by amplifying and sequencing genomic fragments encompassing their known mutations (CAL62: KRAS G12R; C643: HRAS G13R; ACT-1: NRAS Q61K; 8505c: BRAF V600E; OCUT-2: BRAF V600E and PIK3CA H1047R; THJ16T: PIK3CA E545K).

Real-time polymerase chain reaction

Total RNA was extracted with Trizol and reverse transcribed using the Thermoscript kit (Invitrogen, Carlsbad, CA). Quantitative real-time polymerase chain reaction (qRT-PCR) was performed on a StepOne Plus apparatus using the Absolute Blue qPCR Rox Mix (Thermo Scientific, Waltham, MA) and TaqMan expression assays (Applied Biosystems, Carlsbad, CA). Each sample was run in triplicate and *Ipo8* was used to control for input RNA. Data analysis was based on the $\Delta\Delta$ct method, and experiments were repeated at least three times using at least two independent organ pools (at least five mice per pool).

Treatments

GSK461364A was added 24 hours after plating, in quintuplicate. After 72 hours, cell viability was assessed using the Wst-1 assay (Roche Applied Science). Calculation of EC50 values and statistical analysis were done using GraphPad Prism software (version 5.0, GraphPad Software, La Jolla, CA). Preliminary experiments were conducted to ensure that, in the conditions used for these assays, this method yields the same results as direct cell counting (both trypan blue based and automated).

Cell-cycle DNA analysis

The cell lines were seeded in 6-well plates, cultured overnight at 37°C, and incubated for 48 hours with GSK461364A. Cells were harvested by trypsin treatment and fixed in 70% ethanol at −20°C overnight. After treatment with RNase, cells were stained with propidium iodide, and DNA content was measured using a Becton Dickinson LSRII System (BD Biosciences, Franklin Lakes, NJ).

Annexin V staining

The cell lines were seeded in 6-well plates, cultured overnight at 37°C, and incubated for 24–72 hours with GSK461364A. The cell culture supernatant was collected and added to the cells harvested by the trypsin method. Cells were stained with Annexin V FITC and PI (BD Pharmigen, Franklin Lakes, NJ) for 15 minutes at room temperature in the dark. Samples were analyzed by flow cytometry within 1 hour using a Becton Dickinson LSRII System (BD Biosciences).

Immunocytochemistry

Cells were treated at a concentration of GSK461364A corresponding to the IC50 value for 24 hours. They were then fixed with methanol for 15 minutes, permeabilized with Triton X-100 for 5 minutes, blocked in 1% bovine serum albumin for 30 minutes, and incubated with antibodies against α-tubulin (NeoMarkers, Fremont, CA) and Phospho-Histone H3 (Millipore, Temecula, CA) for 2 hours. Alexa fluorophore–conjugated antibodies (Invitrogen) were used as secondary antibodies for detection and 4′,6-diamino-2-phenylindole (DAPI) was used for nuclei detection. Statistical analysis was done using the GraphPad Prism software.

Western blot analysis

Thyroid tissue and cells were homogenized on ice in RIPA buffer supplemented with complete protease inhibitor tablet (Roche Applied Science). Western blot analysis was carried out on 20–40 μg proteins using antibodies from Cell Signaling (Danvers, MA) and a β-actin antibody from Sigma-Aldrich.

In vivo *model*

Female wild-type 129Sv mice (8–10 weeks old; $n=16$) were injected with 6×10^6 T4888M cells, established from a lung metastasis developed by an ATC-positive $[Pten, p53]^{thyr-/-}$ mouse. When tumors reached a size between 100 and 250 mm^3, mice were randomized to GSK461364A treatment (50 mg/kg) or vehicle (2% Cremophor EL, 2% *N*,*N*,-dimethylacetamide in acidified [pH 5] water) groups. GSK461364A was administered via intraperitoneal injection once every other day, and tumor volume was calculated from two-dimensional measurements using the following equation: tumor volume = (length × width^2) × 0.5.

Mice were bled by a retro-orbital puncture, and blood counts were obtained using a Forcyte analyzer (Oxford Science, Oxford, CT).

Statistical analysis

Experiments were performed at least three times. Data were analyzed using Prism software packages. Differences with p-values <0.05 were considered statistically significant.

Results

We have previously described the results of our genome-wide expression profiling of thyroid tissue from wild-type, single- and double-mutant $[Pten, p53]^{thyr-/-}$ mice, compared with five anaplastic carcinomas developed by these compound mutants, using the Affymetrix platform (29). Intersection of the list of genes deregulated in the mouse tumors with comparable datasets generated from human ATCs identified a clear "mitotic signature": 24 of the top 50 common upregulated genes

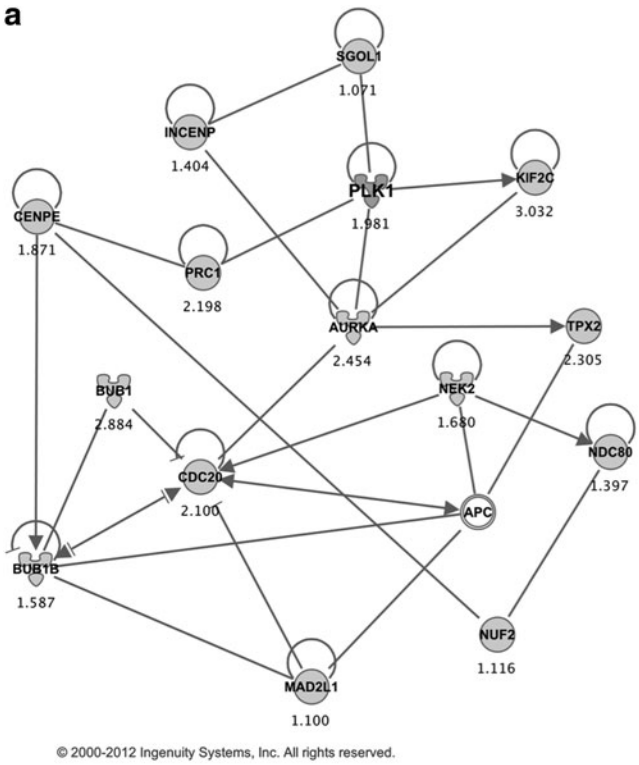

FIG. 1. **(a)** Ingenuity network generated by mapping the genes differentially expressed between tumor and control thyroid tissue. The network is graphically displayed with genes as nodes (different shapes represent the functional classes of the gene products) and the biological relationships between the nodes as lines. A solid line without arrow indicates protein–protein interaction. Arrows indicate the direction of action of one gene to another. **(b, c)** *Plk-1* expression profiling by real-time PCR and protein levels using thyroid pools from 4-month-old control and single-mutant mice, ATC-free, progressively older (4, 6, and 8 months) double mutants, and histologically confirmed ATCs from 8- to 9-month-old double mutants. ATC, anaplastic thyroid carcinoma; PCR, polymerase chain reaction.

Table 1. Comparison of Expression Changes for Mitotic Genes in Anaplastic and Poorly Differentiated Thyroid Carcinomas, Compared to Wild Type Controls

	ATC vs. WT		*PDTC vs. WT*	
	Log FC	*FDR*	*Log FC*	*FDR*
Plk1	2.598	2.79E-06	1.332	0.005
Aurka	2.135	1.39E-06	1.117	0.001
Cdc20	1.952	3.15E-06	1.032	0.002
Mad2l1	1.743	3.07E-06	1.109	0.002
Nek2	1.737	1.88E-06	0.888	0.004
Tpx2	2.700	9.62E-07	1.331	0.002
Ndc80	1.447	1.75E-05	1.286	0.002
Prc1	2.685	7.98E-07	1.644	1.69E-04

ATC, anaplastic thyroid carcinoma; PDTC, poorly differentiated thyroid carcinoma; WT, wild type; FC, fold change; FDR, false discovery rate.

encode for proteins involved in the control of the G2/M transition and of the mitotic process, indicating that murine and human ATCs share a significant mitotic dysfunction (15,29).

Using bioinformatic approaches, we identified *Plk1* as a clinically valuable target at the center of this deregulated mitotic network (Fig. 1a). We next used RT-PCR and Western blotting to measure Plk1 expression levels in control and mutant mice: while mRNA levels of *Plk1* were not significantly altered in single mutants or in compound mutants before the development of frank ATC, a slight increase in protein levels was observed in 8-month-old [*Pten, p53*]$^{thyr-/-}$ compound mutants, when ATC begins to develop (Fig. 1b, c). Conversely, the expression of Plk1 was increased by an average of 20-fold in ATC samples (Fig. 1b, c). These findings validate the expression profiling data and suggest that PLK1 may be a valuable therapeutic target, at least in those ATCs that are driven by PI3K constitutive activation.

Furthermore, PDTCs developing in *Pten*$^{thyr-/-}$,*Kras*^{G12D} mice share the upregulation of most of the genes present in the mitotic signature described above (Table 1), suggesting that this mitotic dysfunction also characterizes PDTCs.

Previous studies have shown that ATC cell lines carrying mutations in the RAS/RAF cascade are sensitive to the PLK inhibitor BI2536 (25). To determine whether and how the nature of the driver mutation would influence the tumor cell sensitivity to PLK1 inhibition with GSK461364A, we selected a panel of mouse and human ATC cell lines encompassing the whole spectrum of mutations commonly observed in primary ATC, and generated dose–response viability curves. This approach clearly showed that both mouse (T1860, T1903) and human [THJ16T (30)] ATC cell lines carrying mutations that activate the PI3K pathway, and human ATC cell lines harboring activating mutations in *BRAF* (8505c), *KRAS* (Cal62), *NRAS* (ACT1), *HRAS* (C643), or in both *BRAF* and *PIK3CA* (Ocut-2) were strongly inhibited by nanomolar doses of GSK461364A (Fig. 2).

Next, we tested whether GSK461364A would also be effective against cell lines derived from PDTCs developing in *Pten*$^{thyr-/-}$, *Kras*^{G12D} mice, T683 and T826. In fact, murine PDTC cells were as sensitive to Plk1 inhibition as ATC cells, with growth suppression achieved in the low nanomolar range (Fig. 2).

PLK1 inhibition leads to a block of the cells in the G2/M phase of the cell cycle, which serves as a marker of an on-target effect (31). We treated our panel of cell lines with GSK461364A at concentrations corresponding to the IC25, IC50, and IC75 for 48 hours and determined their cell cycle profile by flow cytometry. All the ATC cell lines were arrested in G2/M in a dose-dependent manner, and no major differences in the extent of G2/M arrest were found between cell lines harboring different driver mutations. However, all and only the cell lines carrying mutations that activate the PI3K cascade displayed a significant population of tetraploid cells that had escaped the cell cycle arrest and undergone mitotic slippage (Fig. 3).

Immunofluorescence analysis was performed using antibodies against α-tubulin and phospho-histone H3 to identify the mitotic spindle and mitotic DNA, respectively. This experiment further confirmed a solid on-target effect: 20–35% of the cells were positive for phospho-histone H3 and displayed disorganized microtubules and unipolar or multipolar mitotic spindles 24 hours after treatment with GSK461364A at IC75 (Fig. 4a, b).

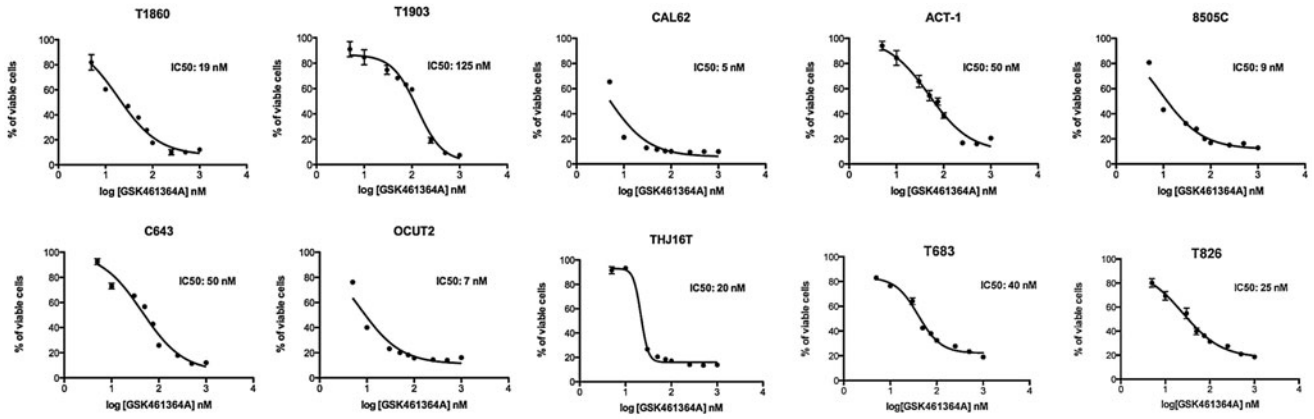

FIG. 2. Dose–response curves showing the effect of GSK461364A on the viability of a panel of ATC and PDTC cell lines (mouse cell lines: T1860, T1903, T683, T826; human cell lines: Cal62, C643, ACT-1, OCUT-2, 8505-C, THJ16T). PDTC, poorly differentiated thyroid carcinoma.

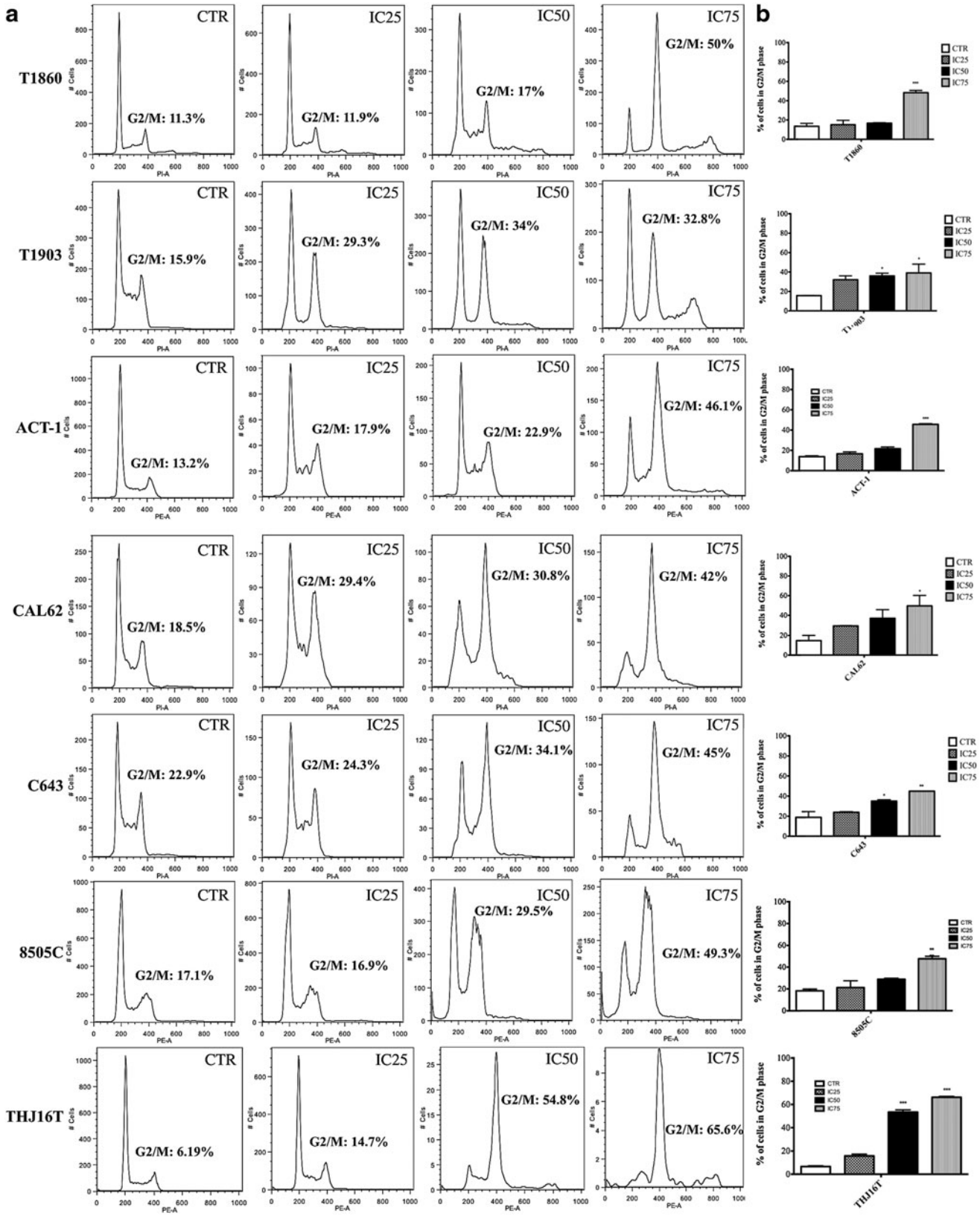

FIG. 3. **(a)** Cell cycle profile of ATC cells exposed to increasing doses of GSK461364A (concentrations corresponding to IC25, IC50, and IC75) for 48 hours. **(b)** Cell cycle analysis quantification: $^{*}p < 0.05$, $^{**}p < 0.01$, $^{***}p < 0.001$.

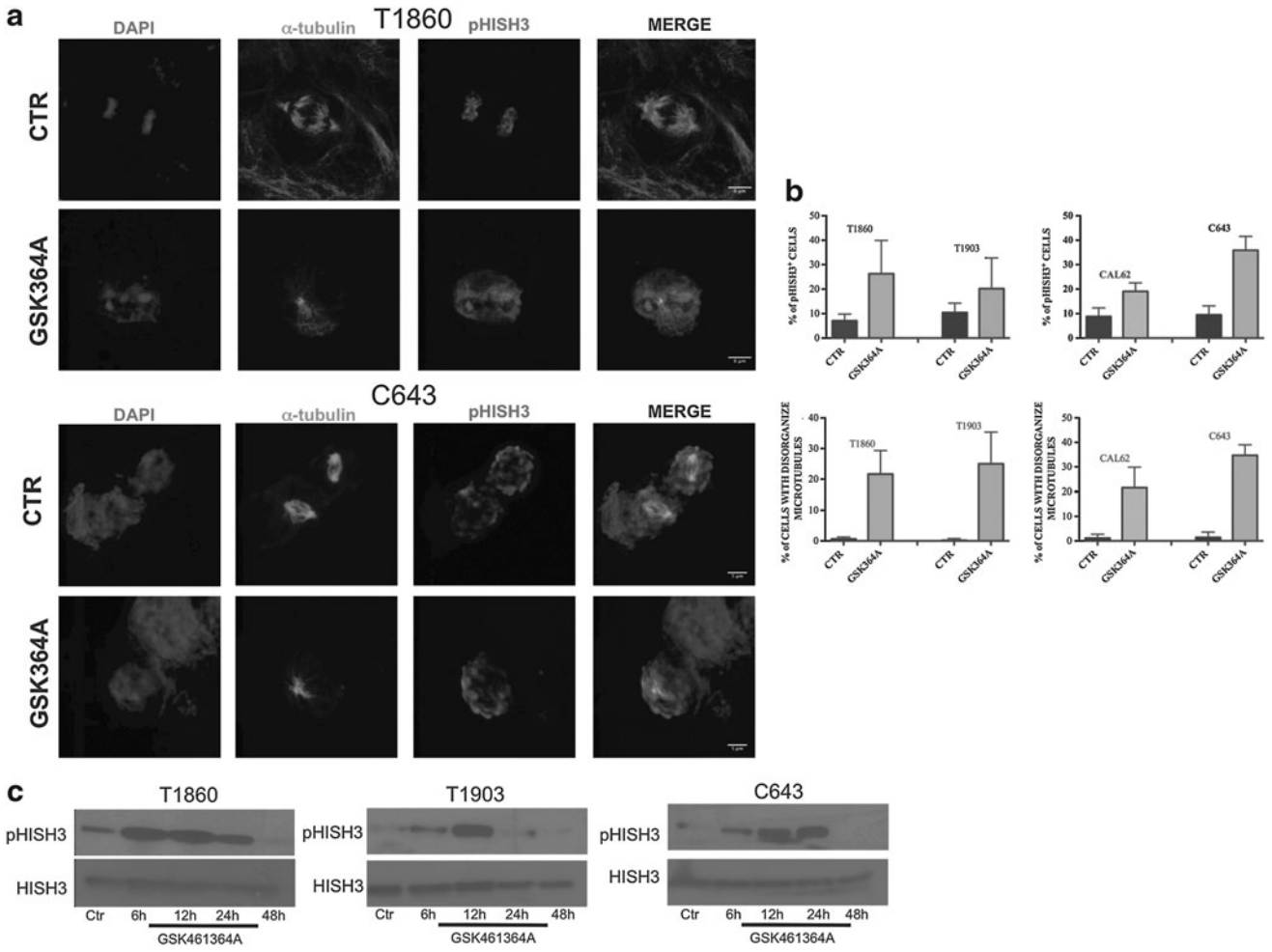

FIG. 4. **(a)** Immunocytochemistry analysis. Cells were fixed and stained after 24 hours of treatment with GSK461364A at IC75 concentration. Cells were stained with DAPI, α-tubulin, and pHISH3. **(b)** Quantification. Top panel: pHISH3-positive cells. Bottom panel: % of microtubules disorganization. **(c)** pHISH3 detection by Western blot. Cells were harvested at different time points after treatment with GSK461364A at IC75 concentration. DAPI, 4′,6-diamino-2-phenylindole.

When we analyzed by Western blotting the levels of phospho-histone H3 at various time-points after GSK461364A treatment (IC75 concentration), we found that the early (at 6–12 hours) increase in phospho-histone H3 levels was followed by a sudden drop between 24 and 48 hours, suggesting that the arrest in G2/M may be followed by mitotic catastrophe and cell death (Fig. 4c). In fact, apoptotic cells were detected by annexin V staining as early as 24 hours after treatment, peaking between 48 and 72 hours (Fig. 5a). Apoptosis was further confirmed by the detection of the cleaved form of caspase 3 about 72 hours after treatment with GSK461364A at IC75 (Fig. 5b). The extent of the apoptotic response among the different cell lines was less homogeneous than that of proliferation inhibition and G2/M arrest; however, it did not correlate with the known genetic alterations present in the different cell lines.

Overexpression of *Mdr1* (*ABCB1*) is often observed in tumors that, like ATCs, display poor response to conventional chemotherapy (32). Accordingly, ATCs developed by [*Pten, p53*]$^{thyr-/-}$ mice express high levels of *Mdr1* mRNA (Fig. 6a). To determine whether a correlation exists between the good response to GSK461364A observed in the panel of mouse and human cell lines used in this study and the levels of expression of *Mdr1*, we performed qRT-PCR to measure *Mdr1* mRNA. We found that our panel included cell lines (both murine and human) with extremely different *Mdr1* levels, suggesting that Mdr1-mediated drug efflux capacity does not affect GSK461364A efficacy (Fig. 6b, c).

Finally, we used an immunocompetent *in vivo* system, that is, 129Sv mice bearing T4888M allograft tumors. T4888M is an ATC cell line generated in our laboratory from a lung metastasis developed by a [*Pten, p53*]$^{thyr-/-}$ compound mutant that had developed ATC. When dosed at 50 mg/kg with a q2dx6 schedule (one dose every other day repeated six times) (27), GSK461364A provided striking tumor control (Fig. 7). Toxicity was limited, with an average 7% body weight loss after one week of treatment.

Although neutrophils, as expected, were reduced in GSK461364A-treated mice compared with controls ($1.87\times10^3/\mu$L vs. $5.94\times10^3/\mu$L), this model was characterized by marked leukocytosis (white blood cells = $15.79\times10^3/\mu$L vs. $1.8–10.7\times10^3/\mu$L normal range), as it is often observed in human ATCs (30). As a consequence, neutrophil counts in the treated mice never fell below normal limits ($0.1–2.4\times10^3/\mu$L).

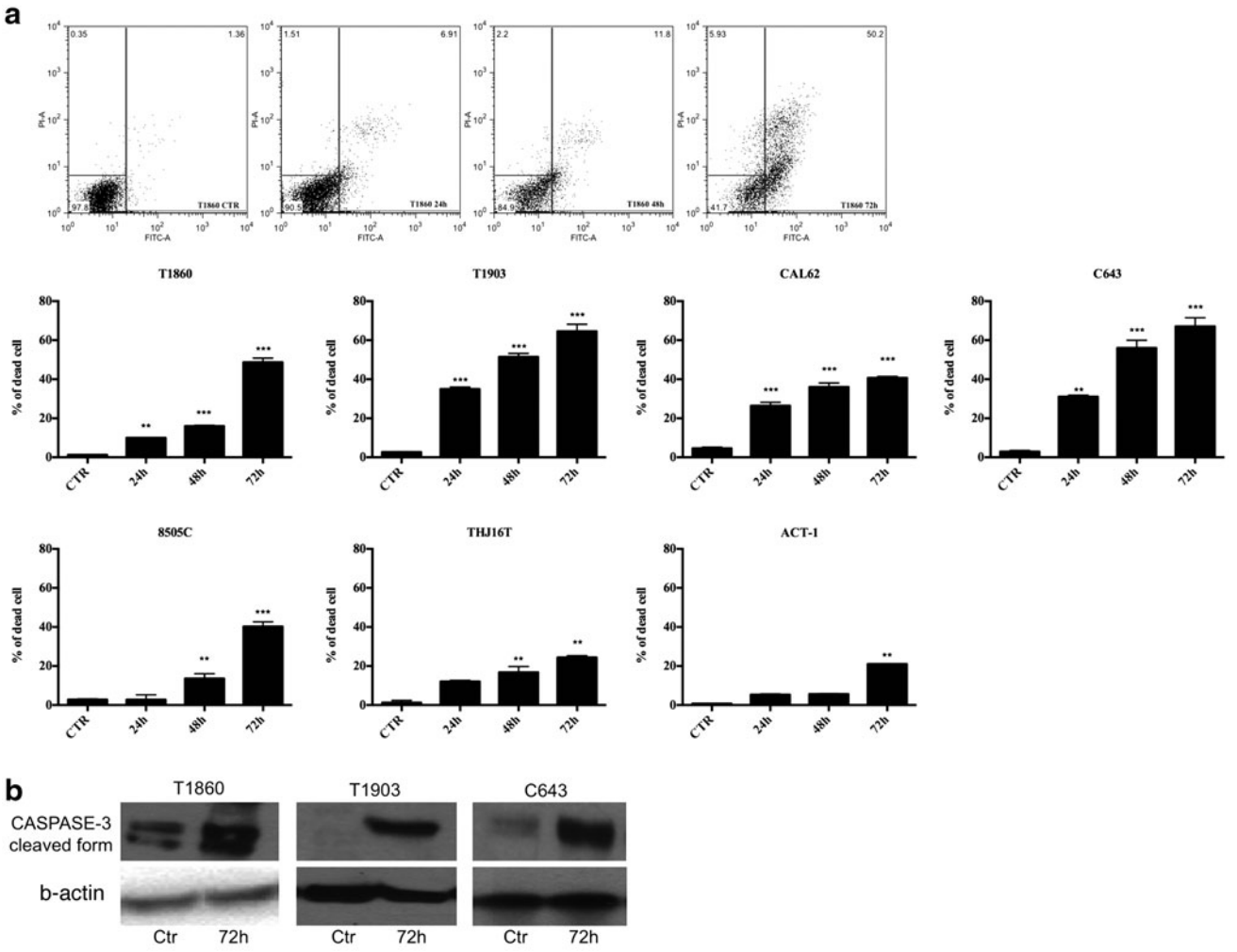

FIG. 5. **(a)** Cells were treated for 24, 48, and 72 hours with GSK461364A at IC75 concentration. At the end of the treatment, cells were stained by annexin V and propidium iodide and analyzed with FACS. $^{**}p < 0.01$, $^{***}p < 0.001$. **(b)** Caspase 3 detection by Western blot after 72 hours of treatment with GSK461364A at IC75 concentration. FACS, fluorescence-activated cell sorting.

Discussion

Anaplastic thyroid cancer patients face a very dismal prognosis, because of the aggressiveness and drug resistance of these tumors. The rarity of the disease and the lack of relevant model systems have long hindered the identification of specific molecular mechanisms and targets that might offer novel and more effective therapeutic approaches.

We have recently reported the generation and characterization of the first autochthonous and immunocompetent

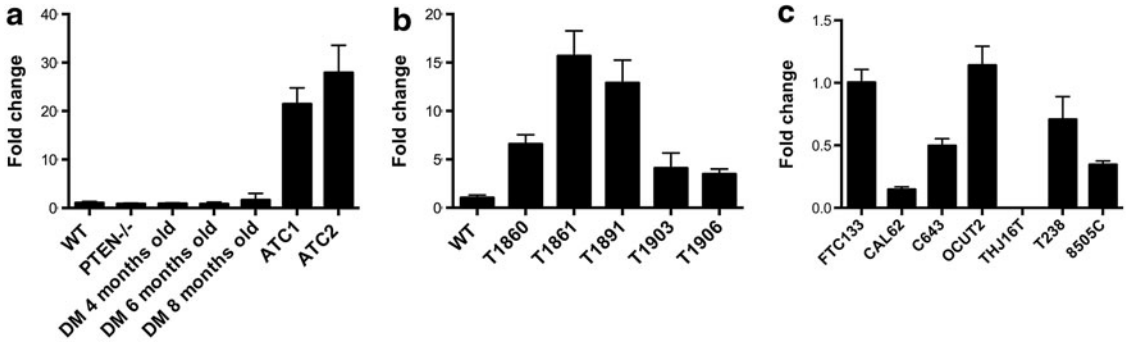

FIG. 6. Mdr-1 expression profiling by real-time PCR in **(a)** thyroid pools from 4-month-old control and single-mutant mice, ATC-free, progressively older (4, 6, and 8 months) double mutants, and histologically confirmed ATCs from 8- to 9-month-old double mutants. **(b)** In $[Pten, p53]^{thyr-/-}$ mouse cell lines. **(c)** In ATC human cell lines.

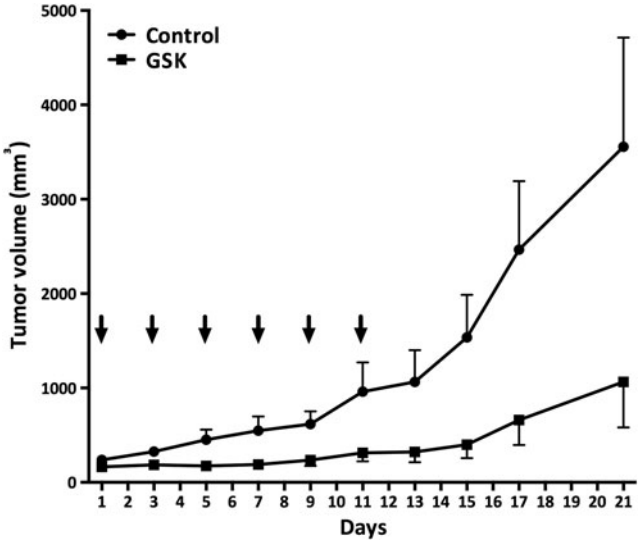

FIG. 7. GSK461364A activity in an allograft tumor model. Tumor volume was determined for GSK461364A (intraperitoneal administration) for a q2dx6 schedule. Arrows indicate drug administration days.

mouse model of ATC (15), a long-needed tool to accelerate and deepen our understanding of this lethal disease. By comparing the gene expression profiles of murine ATCs and PDTCs with available datasets from human ATCs, we have demonstrated in both species the coordinated overexpression of a set of genes involved in the control of mitotic progression. While the finding of increased levels of mitotic regulators and of sensitivity to PLK1 inhibitors in human ATCs is not absolutely novel (10,25), our data, for the first time, extend these notions to the subgroup of PDTCs and ATCs in which PI3K activation represents the driver oncogenic pathway. Thus, the mitotic signature appears to be a general feature of aggressive thyroid tumors, independently of their driver mutation.

Along the same line, our *in vitro* and *in vivo* data provide strong evidence that PLK1 targeting is effective in mouse and human PDTC and ATC cell lines carrying PI3K-activating mutations, in addition to cell lines in which the driver oncogene is *NRAS*, *KRAS*, *HRAS*, or *BRAF*. On the basis of these data and the fact that our PDTC cell lines retain *Tp53* (29), it is possible to speculate that the sensitivity to PLK1 inhibition might actually be dictated not by *TP53* loss or mutation, as previously hypothesized for other tumor types (16), but rather by the high degree of dedifferentiation and the high proliferative index characteristic of these tumors.

In addition, we have shown that sensitivity to PLK1 inhibition does not correlate with the expression of *MDR1*, a key determinant of drug resistance, since both mouse and human cell lines have a range of *MDR1* expression spanning over one log and respond very similarly to GSK461364A.

An important finding of this study is that cell lines with constitutive activation of PI3K show a significant population of cells escaping growth arrest and mitotic catastrophe through mitotic slippage. A similar finding has recently been reported examining the effects of nocodazole in HeLa cells expressing constitutively active AKT (33). High PI3K activity might induce this effect by increasing mitotic exit speed (34,35), or directly protecting cells from mitotic catastrophe (36–38).

The notion that a high percentage of ATCs is characterized by direct or indirect PI3K activation (13) underlines the risk of generating polyploid, genetically unstable cell populations by targeting these tumors with a PLK1 inhibitor.

Furthermore, a recent phase I study of GSK461364A in advanced solid malignancies (20) has shown prolonged stable disease in 15% of patients as the best response achieved, and neutropenia as the most common dose-limiting toxicity.

All together, these data strongly suggest that simultaneous targeting of PLK1 and PI3K might impede the generation of "escaped" polyploid tumor cells while, at the same time, increasing therapeutic efficacy at drug doses that appear so far poorly effective when used as single agents.

Acknowledgments

We wish to thank GlaxoSmithKline for providing GSK461364A, and Dr. J.A. Copland (Mayo Clinic, Jacksonville, FL) for providing the THJ16T cells. This work was supported by NIH Grant CA128943. A.D.C is a recipient of the Irma T. Hirschl Career Scientist Award.

Author Disclosure Statement

No competing financial interests exist.

References

1. Wang HM, Huang YW, Huang JS, Wang CH, Kok VC, Hung CM, Chen HM, Tzen CY 2007 Anaplastic carcinoma of the thyroid arising more often from follicular carcinoma than papillary carcinoma. Ann Surg Oncol **14:**3011–3018.
2. Quiros RM, Ding HG, Gattuso P, Prinz RA, Xu X 2005 Evidence that one subset of anaplastic thyroid carcinomas are derived from papillary carcinomas due to BRAF and p53 mutations. Cancer **103:**2261–2268.
3. Patel KN, Shaha AR 2006 Poorly differentiated and anaplastic thyroid cancer. Cancer Control **13:**119–128.
4. Smallridge RC 2012 Approach to the patient with anaplastic thyroid carcinoma. J Clin Endocrinol Metab **97:**2566–2572.
5. Smallridge RC, Marlow LA, Copland JA 2009 Anaplastic thyroid cancer: molecular pathogenesis and emerging therapies. Endocr Relat Cancer **16:**17–44.
6. Sherman EJ, Lim SH, Ho AL, Ghossein RA, Fury MG, Shaha AR, Rivera M, Lin O, Wolden S, Lee NY, Pfister DG 2011 Concurrent doxorubicin and radiotherapy for anaplastic thyroid cancer: a critical re-evaluation including uniform pathologic review. Radiother Oncol **101:**425–430.
7. Higashiyama T, Ito Y, Hirokawa M, Fukushima M, Uruno T, Miya A, Matsuzuka F, Miyauchi A 2010 Induction chemotherapy with weekly paclitaxel administration for anaplastic thyroid carcinoma. Thyroid **20:**7–14.
8. Ain KB, Egorin MJ, DeSimone PA 2000 Treatment of anaplastic thyroid carcinoma with paclitaxel: phase 2 trial using ninety-six-hour infusion. Collaborative Anaplastic Thyroid Cancer Health Intervention Trials (CATCHIT) Group. Thyroid **10:**587–594.
9. Zheng X, Cui D, Xu S, Brabant G, Derwahl M 2010 Doxorubicin fails to eradicate cancer stem cells derived from anaplastic thyroid carcinoma cells: characterization of resistant cells. Int J Oncol **37:**307–315.
10. Salvatore G, Nappi TC, Salerno P, Jiang Y, Garbi C, Ugolini C, Miccoli P, Basolo F, Castellone MD, Cirafici AM, Melillo RM, Fusco A, Bittner ML, Santoro M 2007 A cell prolifera-

tion and chromosomal instability signature in anaplastic thyroid carcinoma. Cancer Res **67:**10148–10158.
11. Ibrahimpasic T, Ghossein R, Carlson DL, Chernichenko N, Nixon I, Palmer FL, Lee NY, Shaha AR, Patel SG, Tuttle RM, Balm AJ, Shah JP, Ganly I 2013 Poorly differentiated thyroid carcinoma presenting with gross extrathyroidal extension: 1986–2009 Memorial Sloan-Kettering Cancer Center experience. Thyroid **23:**997–1002.
12. Gauchotte G, Philippe C, Lacomme S, Leotard B, Wissler MP, Allou L, Toussaint B, Klein M, Vignaud JM, Bressenot A 2011 BRAF, p53 and SOX2 in anaplastic thyroid carcinoma: evidence for multistep carcinogenesis. Pathology **43:**447–452.
13. Liu Z, Hou P, Ji M, Guan H, Studeman K, Jensen K, Vasko V, El-Naggar AK, Xing M 2008 Highly prevalent genetic alterations in receptor tyrosine kinases and phosphatidylinositol 3-kinase/akt and mitogen-activated protein kinase pathways in anaplastic and follicular thyroid cancers. J Clin Endocrinol Metab **93:**3106–3116.
14. Nikiforov YE 2004 Genetic alterations involved in the transition from well-differentiated to poorly differentiated and anaplastic thyroid carcinomas. Endocr Pathol **15:** 319–327.
15. Antico Arciuch VG, Russo M, Dima M, Kang KS, Dasrath F, Liao XH, Refetoff S, Montagna C, Di Cristofano A 2011 Thyrocyte-specific inactivation of p53 and Pten results in anaplastic thyroid carcinomas faithfully recapitulating human tumors. Oncotarget **2:**1109–1126.
16. Degenhardt Y, Greshock J, Laquerre S, Gilmartin AG, Jing J, Richter M, Zhang X, Bleam M, Halsey W, Hughes A, Moy C, Liu-Sullivan N, Powers S, Bachman K, Jackson J, Weber B, Wooster R 2010 Sensitivity of cancer cells to Plk1 inhibitor GSK461364A is associated with loss of p53 function and chromosome instability. Mol Cancer Ther **9:**2079–2089.
17. Lee SR, Park JH, Park EK, Chung CH, Kang SS, Bang OS 2005 Akt-induced promotion of cell-cycle progression at G2/M phase involves upregulation of NF-Y binding activity in PC12 cells. J Cell Physiol **205:**270–277.
18. Strebhardt K 2010 Multifaceted polo-like kinases: drug targets and antitargets for cancer therapy. Nat Rev Drug Discov **9:**643–660.
19. Petronczki M, Lenart P, Peters JM 2008 Polo on the rise-from mitotic entry to cytokinesis with Plk1. Dev Cell **14:**646–659.
20. Olmos D, Barker D, Sharma R, Brunetto AT, Yap TA, Taegtmeyer AB, Barriuso J, Medani H, Degenhardt YY, Allred AJ, Smith DA, Murray SC, Lampkin TA, Dar MM, Wilson R, de Bono JS, Blagden SP 2011 Phase I study of GSK461364, a specific and competitive Polo-like kinase 1 inhibitor, in patients with advanced solid malignancies. Clin Cancer Res **17:**3420–3430.
21. Vose JM, Friedberg JW, Waller EK, Cheson BD, Juvvigunta V, Fritsch H, Petit C, Munzert G, Younes A 2012 The Plk1 inhibitor BI 2536 in patients with refractory or relapsed non-Hodgkin lymphoma: a phase I, open-label, single dose-escalation study. Leuk Lymphoma **54:**708–713.
22. Frost A, Mross K, Steinbild S, Hedbom S, Unger C, Kaiser R, Trommeshauser D, Munzert G 2012 Phase i study of the Plk1 inhibitor BI 2536 administered intravenously on three consecutive days in advanced solid tumours. Curr Oncol **19:**e28–e35.
23. Jimeno A, Li J, Messersmith WA, Laheru D, Rudek MA, Maniar M, Hidalgo M, Baker SD, Donehower RC 2008 Phase I study of ON 01910.Na, a novel modulator of the Polo-like kinase 1 pathway, in adult patients with solid tumors. J Clin Oncol **26:**5504–5510.
24. Shi JQ, Lasky K, Shinde V, Stringer B, Qian MG, Liao D, Liu R, Driscoll D, Nestor MT, Amidon BS, Rao Y, Duffey MO, Manfredi MG, Vos TJ, N DA, Hyer ML 2012 MLN0905, a small-molecule plk1 inhibitor, induces antitumor responses in human models of diffuse large B-cell lymphoma. Mol Cancer Ther **11:**2045–2053.
25. Nappi TC, Salerno P, Zitzelsberger H, Carlomagno F, Salvatore G, Santoro M 2009 Identification of Polo-like kinase 1 as a potential therapeutic target in anaplastic thyroid carcinoma. Cancer Res **69:**1916–1923.
26. Griffith OL, Melck A, Jones SJ, Wiseman SM 2006 Meta-analysis and meta-review of thyroid cancer gene expression profiling studies identifies important diagnostic biomarkers. J Clin Oncol **24:**5043–5051.
27. Gilmartin AG, Bleam MR, Richter MC, Erskine SG, Kruger RG, Madden L, Hassler DF, Smith GK, Gontarek RR, Courtney MP, Sutton D, Diamond MA, Jackson JR, Laquerre SG 2009 Distinct concentration-dependent effects of the polo-like kinase 1-specific inhibitor GSK461364A, including differential effect on apoptosis. Cancer Res **69:** 6969–6977.
28. Miller KA, Yeager N, Baker K, Liao XH, Refetoff S, Di Cristofano A 2009 Oncogenic Kras requires simultaneous PI3K signaling to induce ERK activation and transform thyroid epithelial cells *in vivo*. Cancer Res **69:**3689–3694.
29. Dima M, Miller KA, Antico-Arciuch VG, Di Cristofano A 2011 Establishment and characterization of cell lines from a novel mouse model of poorly differentiated thyroid carcinoma: powerful tools for basic and preclinical research. Thyroid **21:**1001–1007.
30. Sugitani I, Miyauchi A, Sugino K, Okamoto T, Yoshida A, Suzuki S 2012 Prognostic factors and treatment outcomes for anaplastic thyroid carcinoma: ATC Research Consortium of Japan cohort study of 677 patients. World J Surg **36:**1247–1254.
31. Hikichi Y, Honda K, Hikami K, Miyashita H, Kaieda I, Murai S, Uchiyama N, Hasegawa M, Kawamoto T, Sato T, Ichikawa T, Cao S, Nie Z, Zhang L, Yang J, Kuida K, Kupperman E 2011 TAK-960, a novel, orally available, selective inhibitor of Polo-like kinase 1, shows broad-spectrum preclinical antitumor activity in multiple dosing regimens. Mol Cancer Ther **11:**700–709.
32. Sugawara I, Masunaga A, Itoyama S, Sumizawa T, Akiyama S, Yamashita T 1995 Expression of multidrug resistance-associated protein (MRP) in thyroid cancers. Cancer Lett **95:**135–138.
33. Xiong F, Lin Y, Han Z, Shi G, Tian L, Wu X, Zeng Q, Zhou Y, Deng J, Chen H 2012 Plk1-mediated phosphorylation of UAP56 regulates the stability of UAP56. Mol Biol Rep **39:**1935–1942.
34. Lu J, Tan M, Huang WC, Li P, Guo H, Tseng LM, Su XH, Yang WT, Treekitkarnmongkol W, Andreeff M, Symmans F, Yu D 2009 Mitotic deregulation by survivin in ErbB2-overexpressing breast cancer cells contributes to Taxol resistance. Clin Cancer Res **15:**1326–1334.
35. Stiles B, Gilman V, Khanzenzon N, Lesche R, Li A, Qiao R, Liu X, Wu H 2002 Essential role of AKT-1/protein kinase B alpha in PTEN-controlled tumorigenesis. Mol Cell Biol **22:**3842–3851.
36. Hirose Y, Katayama M, Mirzoeva OK, Berger MS, Pieper RO 2005 Akt activation suppresses Chk2-mediated, methylating agent-induced G2 arrest and protects from temozolomide-induced mitotic catastrophe and cellular senescence. Cancer Res **65:**4861–4869.

37. Hemstrom TH, Sandstrom M, Zhivotovsky B 2006 Inhibitors of the PI3-kinase/Akt pathway induce mitotic catastrophe in non-small cell lung cancer cells. Int J Cancer **119:**1028–1038.
38. Koul D, Fu J, Shen R, Lafortune TA, Wang S, Tiao N, Kim YW, Liu JL, Ramnarian D, Yuan Y, Garcia-Echevrria C, Maira SM, Yung WK 2012 Antitumor activity of NVP-BKM120—a selective pan class I PI3 kinase inhibitor showed differential forms of cell death based on p53 status of glioma cells. Clin Cancer Res **18:**184–195.

Address correspondence to:
Antonio Di Cristofano, PhD
Department of Developmental and Molecular Biology
Price Center for Genetic and Translational Medicine
Albert Einstein College of Medicine
1301 Morris Park Avenue, Room 302
Bronx, NY 10461

E-mail: antonio.dicristofano@einstein.yu.edu